

Shape parameters of the solar corona from 1991 to 2016

Rhorom Priyatikanto

¹ Astronomy Program, Faculty of Mathematics and Natural Sciences, Institut Teknologi Bandung, Bandung 40132, Indonesia

² Space Science Center, National Institute of Aeronautics and Space, Bandung 40173, Indonesia;
rhrom.priyatikanto@lapan.go.id

Received 2016 May 26; accepted 2016 July 27

Abstract The global structure of the solar corona observed in the optical window is governed by the global magnetic field with different characteristics over a solar activity cycle. The Ludendorff flattening index has become a popular measure of global structure of the solar corona as observed during an eclipse. In this study, 15 digital images of the solar corona from 1991 to 2016 were analyzed in order to construct coronal flattening profiles as a function of radius. In most cases, the profile can be modeled with a 2nd order polynomial function so that the radius with maximum flattening index (R_{\max}) can be determined. Along with this value, Ludendorff index ($a + b$) was also calculated. Both Ludendorff index and R_{\max} show anti-correlation with monthly sunspot number, though the R_{\max} values are more scattered. The variation in R_{\max} can be regarded as the impact of the changing coronal brightness profile over the equator.

Key words: Sun: corona — Sun: activity — methods: observational

1 INTRODUCTION

The corona is the outer part of the solar atmosphere. It has a density of $\sim 10^{15} \text{ m}^{-3}$ and a temperature of millions of Kelvin. This layer has a total brightness of about 4×10^{-6} times that of the solar photosphere (Hanaoka et al. 2012) making it only observable in short wavelengths (extreme ultraviolet and X-ray) or when the glaring photosphere is blocked by a coronagraph or the lunar disk during a solar eclipse. Therefore, the relatively rare occurrence of total solar eclipses provides an opportunity to study the solar corona in the optical window (or white light) from the ground. In this window, the corona can be categorized into a K (*kontinuerlich*) corona or an F (*Fraunhofer*) corona which have different properties. Continuum radiation from the K corona, which dominates the inner part ($r < 2 R_{\odot}$), is caused by Thompson scattering of photospheric radiation by electrons in the corona. In the outer part, interplanetary dust scatters the Sun's radiation and creates an F corona (Foukal 2004).

The global structure of the solar corona observed in the optical window represents the electron distribution in this layer, which is influenced by local and global magnetic fields extending from the photosphere to the corona (e.g. Sýkora et al. 2003; Pasachoff et al. 2009). The change in coronal structure or shape over the solar activity cycle is clearly observed. During minimum, there are few active regions and helmet streamers are relatively concentrated near the equator so that the corona tends to be flattened. Conversely, the solar corona becomes more radially

symmetric during the maximum phase as the streamers are more evenly distributed over heliographic latitudes.

Quantitative parameters were defined to describe the global structure of the solar corona, which include the photometric or Ludendorff flattening index (Ludendorff 1928), the geometric flattening index (Nikolsky 1956), angular extent of streamer-free polar regions (Loucif & Koutchmy 1989), the modified flattening index (taking magnetic tilt into account, Gulyaev 1997), and latitudinal span of the helmet streamers (Tlatov 2010). Among these parameters, the Ludendorff index has become the most popular measure and is regularly obtained from coronal observations during solar eclipses (Pishkalo 2011). This index can be regarded as the flattening of the solar corona at a heliocentric distance of $2 R_{\odot}$. Values of the Ludendorff index range from ~ 0 during solar maximum to ~ 0.4 during solar minimum.

Pishkalo (2011) has already compiled values of the Ludendorff index from 1851 to 2010 and demonstrated the correlation between this index and monthly sunspot number (SSN). However, rather scattered data obscure this correlation. A similar problem occurred due to variation of flattening index as a function of solar activity phase. From a particular eclipse event, some observers may get different flattening indices. This difference arises from several influencing factors such as observational bias (Sykora et al. 1999), diverse detector characteristics (e.g. film emulsion), exposure time, number of isophotal contours used to calculate flattening index, a poorly-oriented image, and the dif-

ferent statistics implemented (Pishkalo 2011). These factors can be minimized or even eliminated by implementing a homogeneous method of analysis which is the main focus of this study.

The objectives of this study are to re-analyze publicly available coronal images from solar eclipses that occurred from 1991 to 2016 and to construct radial profiles of the flattening index. From each profile, R_{\max} that represents the equatorial radius with maximum flattening index can be determined so that variation of this value over the solar cycle can be examined together with the Ludendorff index. The data used and method applied in this study are explained in Section 2, while the results and discussion are presented in Section 3. This study concludes in Section 4.

2 DATA AND METHOD

For the present study, 15 8-bit solar coronal images with .jpg extension taken during total solar eclipses that occurred from 1991 to 2016 were compiled from various sources. The year 1991 was chosen as a starting point because more observers, both amateurs and professionals, began to share their images via online media. A list of total solar eclipses was compiled from *Fifty Year Canon of Solar Eclipses, 1986–2035* (Espenak 1989). In the 26 year time span from 1991 to 2016, there were 17 total solar eclipses (excluding hybrids) but no appropriate coronal images from the events on 1992 June 30 and 2003 November 23 were found. The path of totality of these two eclipses passed over remote, unpopulated areas.

Except for coronal images from the last eclipse (2016 March 9), the images were downloaded from online publication media with the help of a web browser. Figure 1 displays the inverted images while Table 1 summarizes information related to these images. To ensure data homogeneity, some criteria were implemented in image selection. First, the coronal image should have been acquired using a digital camera equipped with a neutral density filter. The images obtained using a radially graded filter were not selected because this filter enhances the outer part of the solar corona and changes the brightness profile. The second criterion concerns the observational field of view that is localized around 2 to 3 times the Sun’s angular diameter. With this condition, pixel resolution is sufficiently good so that the following analysis can be conducted for the outer corona. Saturated images were obviously discarded.

The first step after downloading the images was to determine the orientation of the solar disk according to the reference images published in some literatures (see Table 1). The exact orientation of the solar pole is very important for analysis of the global structure of the corona. The next process was to extract the brightness profile of the corona as a function of radius (e.g. counts versus radius, see Fig. 2), especially at angles of 0° , $0^\circ \pm 22.5^\circ$, 180° and $180^\circ \pm 22.5^\circ$ that represent equatorial directions and also 90° , $90^\circ \pm 22.5^\circ$, 270° and $270^\circ \pm 22.5^\circ$ that represent polar directions. The resulting profiles will be used to calculate the coronal flattening index as defined by the

following formula

$$\epsilon \equiv \frac{d_0 + d_1 + d_2}{D_0 + D_1 + D_2} - 1, \quad (1)$$

where d_0 , d_1 and d_2 are coronal diameters in equatorial directions, while D_0 , D_1 and D_2 are measured diameters in polar directions. The diameter is just the sum of two opposite radii with specific pixel counts and it is deduced from the previously constructed brightness profile. The values of ϵ range from 0.0 to 0.4, depending on the phase of solar activity (and some other factors). Typically, the flattening index increases with radius in the inner corona (up to $R_{\max} = 1.5 - 2.5 R_\odot$) and then declines to a minimum value. Previous authors often created isophotal contours of the solar corona and calculated flattening index in each contour, but in this study a continuous brightness profile was used to determine the index in smaller intervals of the radius. In this way, the uncertainty in the flattening index can be calculated using a simple rule of error propagation. Large dispersion in brightness profile tends to produce larger uncertainty in the flattening index. Finally, the resulting plot of flattening index versus equatorial radius can be regarded as a flattening profile of the solar corona.

Following the typical increase and decrease of flattening index over equatorial radius (r), it is possible to model the flattening profile using a 2nd order polynomial function. This type of fitting was applied to the data, particularly in the range of $r \leq 3R_\odot$. This restriction is necessary since the error in ϵ increases with radius or the drop of coronal brightness. In addition, statistical weighting was applied in order to get a more robust fitting. Based on this fitting, the radius with maximum flattening index (R_{\max}) and its uncertainty can be obtained.

The value of R_{\max} was used as the structural boundary between the inner and outer corona. The flattening index of the inner part can be modeled using the linear function

$$\epsilon = a + b \left(\frac{r}{R_\odot} - 1 \right) \quad (2)$$

and the summation of the two coefficients in the regression represents the Ludendorff flattening index which is defined as coronal flattening at $r = 2R_\odot$. Additionally, the uncertainty in the Ludendorff index was calculated according to uncertainties in the two coefficients.

3 RESULT AND DISCUSSION

3.1 Flattening Profile

The compiled eclipse images that enclose the corona up to $2-3 R_\odot$ (a bit inside the field of view of *SOHO/LASCO C2*) enable the coronal flattening profile to be constructed as a function of equatorial radius. The resulting profiles from 15 eclipse cases are presented in Figure 3, while shape parameters which consist of R_{\max} and the Ludendorff index are summarized in Table 2. Compiled indices from literatures are also presented as the main comparison together with solar activity phase as defined in

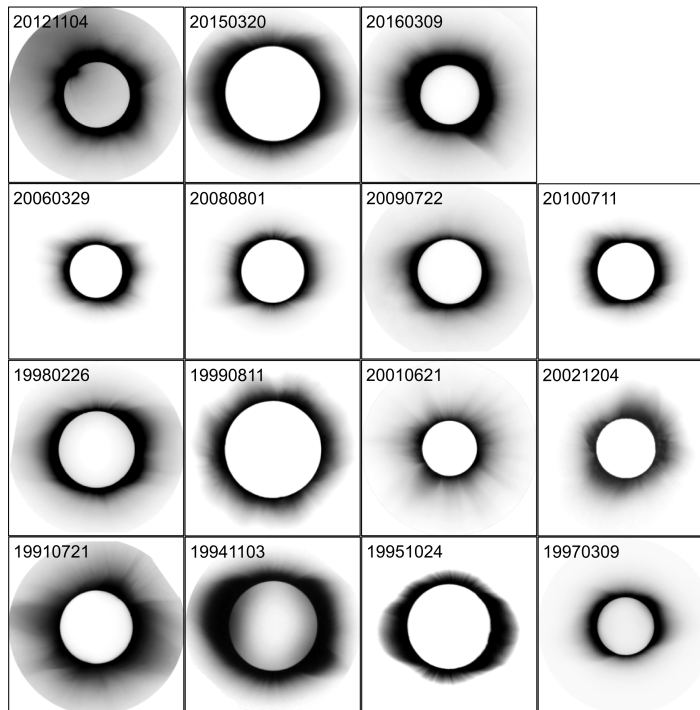


Fig. 1 Inverted images of the solar corona which were obtained during solar eclipses from 1991 to 2016. Each image was cropped into a circular shape so that image rotation was easier.

Table 1 Some Information Related to the Coronal Images Used in This Study

Date	Obs. Site	Observer	Source	Reference Image
1991–07–11	Baja California, Mexico	M.A. Stecker	http://mstecker.com/pages/astse_anr28se1b.htm	Sykora et al. (1999)
1994–11–03	Chile	M. Mobberley	http://martinmobberley.co.uk/TSE.html	Badalyan & Sýkora (2008)
1995–10–24	Ghanoli, India	G. Schneider	http://nicosis.as.arizona.edu:8000/ECLIPSE_WEB/ECLIPSE_95/UMBGRAPHILE_DEBUT_1995.html	Rusin et al. (1996)
1997–03–09	Chita, Russia		https://commons.wikimedia.org/w/index.php?curid=24398440	Pinter et al. (1997)
1998–02–26	Aruba	C.J. Lancaster	http://carllancaster.com/eclipse.htm	Dorotovic et al. (1999)
1999–08–11	Turkey	R.C. Hoagland	http://yowusa.com/nostradamus/KOT_home/KOT/hoagland_rebuttal/hoagland_rebuttal.shtml	Badalyan & Sýkora (2008)
2001–06–21	Lusaka, Zambia	W. Carlos	http://web.williams.edu/Astronomy/eclipse/eclipse2001/2001total/	Reginald et al. (2003)
2002–12–04	Ceduna, Australia	J. Pasachoff et al.	https://svs.gsfc.nasa.gov/cgi-bin/details.cgi?aid=2655	
2006–03–29	Tokat, Turkey	K. Kulac	https://upload.wikimedia.org/wikipedia/commons/2/23/Total_solar_eclipse_2006-04-29.JPG	Pasachoff et al. (2007); Stoeva et al. (2008)
2008–08–01	Novosibirsk, Russia	M. Pozojevic	http://www.hraastro.com/SolarEclipse2008_Novosibirsk/	Pasachoff et al. (2009); Skomorovsky et al. (2012)
2009–07–22	Varanasi, India	M. Dayyala	https://commons.wikimedia.org/wiki/File:Total_solar_eclipse_on_22nd_July_at_Varanasi,India.jpg	Pasachoff et al. (2011a)
2010–07–11	Polynesia	C. Bowden	http://www.weymouthastronomy.co.uk/gallery/eclipse/eclipse.php?show=2	Pasachoff et al. (2011b)
2012–11–13	Australia	NCAR/HAO	https://www2.ucar.edu/for-staff/update/eclipse-12-making-mini-megamovie	Pasachoff et al. (2015)
2015–03–20	Scotland	W.E. Macduff	https://crashmacduff.files.wordpress.com/2015/03/tse.jpg	Bazin et al. (2015)
2016–03–09	Sigi, Indonesia	A. Rachman		Dani et al. (2016)

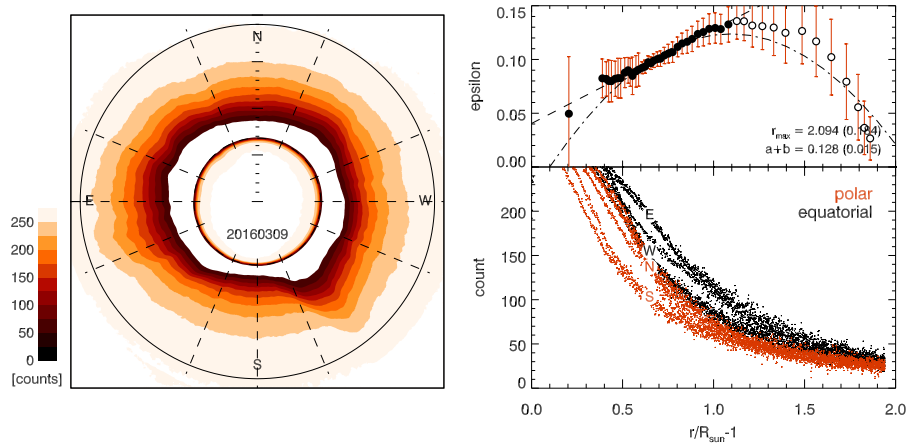


Fig. 2 An example of shape analysis for the coronal image taken during the 2016 March 9 solar eclipse. The left panel displays brightness contours of the corona and the dashed lines mark twelve directions in which brightness profiles were extracted. The bottom right panel shows brightness profiles extracted in equatorial (*dark-color*) and polar (*light-color*) directions. Several groupings are observed due to the asymmetric shape of the corona. Profiles in the north, east, south and west directions are marked accordingly. The top right panel shows the obtained flattening indices and their errors at different equatorial radii, together with the fitted quadratic (*dot-dashed lines*) and linear (*dashed lines*) functions. In this panel, all of the circles represent the data used for 2nd order polynomial fitting, and filled circles are used for linear fitting.

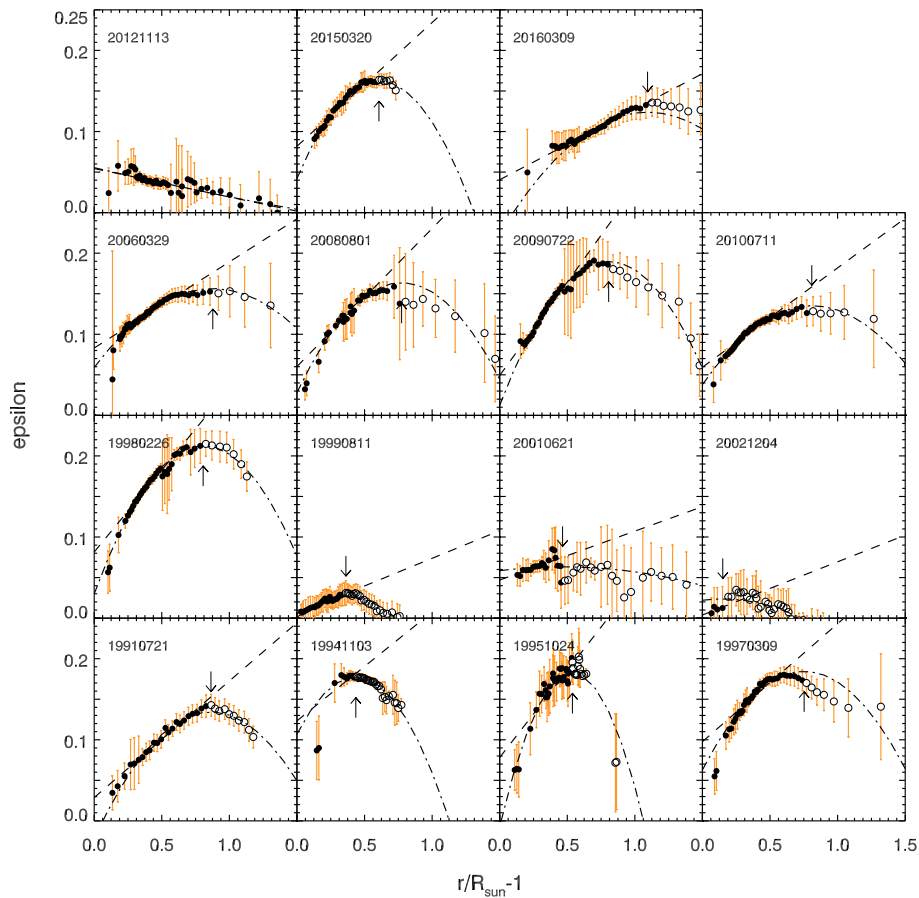


Fig. 3 Flattening profile (ϵ as a function of radius) produced from various coronal images. A quadratic function (*dot-dashed*) was fitted to the data to obtain radius with maximum ϵ (R_{\max}). Data with $r \leq R_{\max}$ (*filled circles*) were used in linear regressions (*dashed*) to determine the Ludendorff index.

Table 2 Summary of the shape parameters (R_{\max} and $a + b$) obtained in this study together with their uncertainties. The corresponding phases of solar activity (Φ) and flattening indices from various literatures are also presented.

Date	Φ	R_{\max} [R_{\odot}]	$\sigma_{R_{\max}}$ [R_{\odot}]	$a + b$	σ_{a+b}	$a + b$ from literatures	
1991-07-21	-0.70	1.86	0.18	0.17	0.02	0.00	Sykora et al. (1999)
1994-11-03	-0.22	1.44	0.16	0.26	0.09	0.14	Badalyan & Sýkora (2008)
1995-10-24	-0.09	1.54	0.11	0.29	0.03	0.28	Rusin et al. (1996)
1997-03-09	0.22	1.75	0.09	0.24	0.01	0.20	Pinter et al. (1997)
1998-02-26	0.48	1.81	0.10	0.28	0.01	0.21	Dorotovic et al. (1999)
1999-08-11	0.87	1.36	0.12	0.07	0.02	0.04	Pishkalo (2011)
2001-06-21	-0.83	1.47	0.70	0.11	0.04	0.07	Pishkalo (2011)
2002-12-04	-0.64	1.15	0.27	0.07	0.39	0.09	Pishkalo (2011)
2006-03-29	-0.22	1.88	0.15	0.19	0.01	0.17	Pishkalo & Sadovenko (2008)
2008-08-01	0.09	1.77	0.09	0.23	0.01	0.21	Pishkalo & Baransky (2009)
2009-07-22	0.25	1.81	0.07	0.28	0.01	0.24	Pishkalo (2011)
2010-07-11	0.40	1.81	0.12	0.18	0.01	0.24	Pishkalo (2011)
2012-11-04	0.77	1.30	0.50	0.02	0.01	0.01	Pasachoff et al. (2015)
2015-03-20	-0.79	1.61	0.12	0.23	0.01	-	
2016-03-09	-0.60	2.09	0.18	0.13	0.02	-	

Ludendorff (1928), e.g. $\Phi = (T_{\text{ecl}} - T_{\text{min}})/|T_{\text{max}} - T_{\text{min}}|$, where T_{ecl} is the time of eclipse, while T_{max} and T_{min} are the times of maximum and minimum in solar activity when T_{ecl} occurred.

As shown in Figure 3, in most cases (80% of the sample) the flattening profile obviously indicates rise and fall that fit sufficiently well with the quadratic function. From this fitting, flattening indices reach maximum values R_{\max} that range between 1.2 and 2.1 R_{\odot} with typical uncertainties below 0.2 R_{\odot} . The largest value is $R_{\max} = 2.09 R_{\odot}$ which was obtained from the last solar eclipse (2016 March 9). In this case, the flattening profile shows a strong linear increase up to R_{\max} and then sharply declines at larger radii. A rather flat brightness profile at large radii produces larger uncertainty in this range. However, by employing statistical weighting, an acceptable quadratic function of the flattening profile can be obtained.

There are two cases where quadratic functions do not fit the flattening profiles well and the implemented method fails to determine a reasonable value of R_{\max} . They are the solar corona associated with solar eclipses that were observed on 2001 June 21 and 2012 November 13. Both eclipses occurred during the maximum phase of solar activity during which the Sun exhibited more helmet streamers. For the former case, streamers and coronal rays radiated from almost all heliographic latitudes such that the solar corona appeared to have a low flattening index. Pishkalo (2011) obtained the Ludendorff index of $a + b = 0.07$ from a white-light portrait of the 2001 solar corona, but this study found a bit higher value, $a + b = 0.11$. In general, there is a declining trend of flattening index though fluctuations are observed and the values at the outer part have larger uncertainties. If the area being examined has a small radius, one may realize that the flattening profile reaches a maximum at approximately $r = 1.5 R_{\odot}$, and then declines slightly. In this case, statistical weighting is crucial and the obtained value of $R_{\max} \approx 1.5 R_{\odot}$ and $a + b \approx 0.11$ are sufficiently convincing.

A similar pattern is observed in the flattening profile of the 2012 coronal image. The flattening index decreases monotonically to the minimum allowed value such that $a + b = 0.02$ was derived. The polynomial fitting algorithm gave a parabolic curve directed upward since there are two data points with a positive trend at large equatorial radius. This fitting is invalid. At small radius, the flattening index cannot be calculated because of saturated pixels. However, the produced flattening profile and determined Ludendorff index are in agreement with the result of Pasachoff et al. (2015) who obtained $a + b = 0.01$. Visual inspection may lead to an approximated value of $R_{\max} = 1.3 R_{\odot}$ since ϵ reaches its maximum at this radius.

3.2 Changes in Shape Parameters Over Solar Cycles

As summarized in Table 2, Ludendorff flattening indices obtained from coronal images taken during solar eclipses that occurred from 1991 to 2016 have values in the range of 0.02 to 0.29, while the radii of maximum flattening vary from 1.20 to 2.09 R_{\odot} . Both shape parameters change over time in phase during the 11-year solar activity cycle (Fig. 4). The shape parameters as a function of solar activity phase (Φ) are also presented in Figure 5. As reviewed by some authors (e.g. Loucif & Koutchmy 1989; Golub & Pasachoff 2009; Pishkalo 2011), Ludendorff flattening index anti-correlates with SSN. During the minimum phase of solar activity ($\Phi \approx 0$), observers tend to observe a flattened corona with larger Ludendorff index and observe a circular corona during maximum ($|\Phi| \approx 1$). Moreover, the latitudinal extension of streamer-free polar regions becomes smaller during solar maximum (Loucif & Koutchmy 1989). Figure 4 also shows that R_{\max} changes in a similar way as the flattening index.

Compared to the change in Ludendorff index, the cyclical variation of R_{\max} is obscured by large dispersion at $\Phi \approx -0.7$. R_{\max} that was obtained from 1991, 2001, 2015 and 2016 can be regarded as deviating cases if an

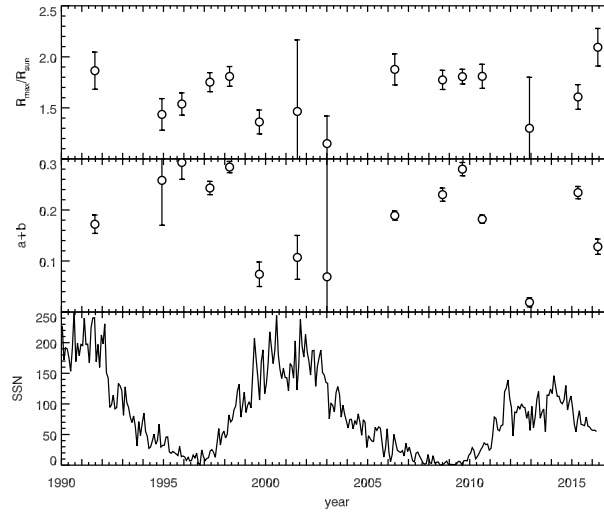


Fig. 4 Variation of shape parameters over the solar activity cycle. The top panel displays R_{\max} over time, while the middle panel shows the Ludendorff flattening index ($a + b$). Monthly average SSN is plotted for comparison in the bottom panel.

11-year cycle is expected. For 1991, the deviation also occurred in the Ludendorff index and might be related to the flattened corona that has been discussed by Sykora et al. (1999). They doubted the definition of the Ludendorff flattening index with its regular change over the solar cycle by arguing that the projected position of the helmet streamer on the celestial plane influences the appearance of the solar corona, and, in turn, the observed shape and flattening. Due to the Carrington rotation lasting 2–3 days, the observed flattening index may change drastically. This can be considered as the source of intrinsic scatter in flattening index over the solar activity cycle. For the case of the 2001 solar eclipse, solar activity was at a maximum level and helmet streamers were distributed almost evenly in every direction (see Fig. 1). The constructed flattening profile is somewhat flat with scatter at large radii. These conditions make the fitting a bit difficult. On the other hand, the last two cases (2015 and 2016 eclipses) correspond to well-defined flattening profiles with relatively large R_{\max} (see Fig. 3).

The R_{\max} value and its variation over the solar cycle are rarely discussed in literatures. The following explanation is proposed to interpret this shape parameter and its change. It starts from the fact that the brightness of the solar corona (K+F) in both equatorial and polar directions declines as the electron density drops exponentially (Newkirk 1967; Badalyan 1996). However, the declining rate in the polar direction is a bit higher (steeper) compared to the one in the equatorial direction (Lebecq et al. 1985; Hanaoka et al. 2012). Although the coronal oblateness arises from the absolute difference between polar and equatorial brightness profiles, the difference among declining rates causes variation in the flattening index along solar distances. Flattening indices increase at $r < R_{\max}$ and decrease at $r > R_{\max}$. The value of R_{\max} may change due to the change in brightness profile of the corona.

Badalyan (1996) examined white-light coronal images taken from 1952 to 1983 and found that the density pa-

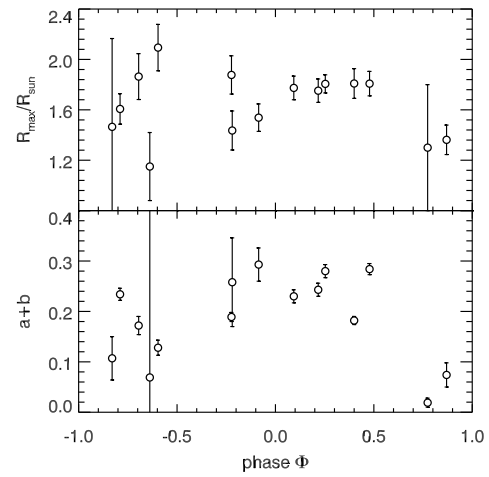


Fig. 5 Shape parameters as a function of phase Φ of solar activity.

rameter of the solar corona (n_0) in the equatorial direction (assuming hydrostatic equilibrium) varies from $2 \times 10^8 \text{ cm}^{-3}$ at the minimum phase of the solar cycle to $4 \times 10^8 \text{ cm}^{-3}$ during maximum. However, n_0 in the polar direction fluctuates around $1 \times 10^8 \text{ cm}^{-3}$ with insignificant amplitude over the solar activity cycle. The discrepancy between equatorial change and polar change may explain the variation of R_{\max} that depends on the solar activity cycle.

4 CONCLUSIONS

In this study, 15 white-light solar coronal images, which were taken during solar eclipses that occurred from 1991 to 2016, have been analyzed using a semi-autonomous method such that the shape parameter of the corona can be determined. Flattening profiles as a function of radius for images have been produced. In most cases (80% of the sample), the flattening profile can be modeled using a 2nd order polynomial function such that the radius of

maximum flattening (R_{\max}) can be determined. At small heliocentric distances ($r \leq R_{\max}$), the flattening index increases almost linearly and the Ludendorff index (flattening at $r = 2 R_{\odot}$) can be extrapolated. In agreement with previous studies, the Ludendorff index anti-correlates with monthly SSN. Additionally, this study shows that R_{\max} changes over the solar cycle in phase with variation of the flattening index. The change of R_{\max} can be interpreted as the observational consequences of the change in equatorial brightness profile that is different from the brightness profile in the polar direction.

Acknowledgements The author thanks the observers who shared coronal images that were analyzed in this study. He also acknowledges Tiar Dani who introduced the study of solar corona structure, particularly related to the total solar eclipse that occurred on 2016 March 9.

References

- Badalyan, O. G. 1996, *Astronomical and Astrophysical Transactions*, 9, 205
- Badalyan, O. G., & Sýkora, J. 2008, *Contributions of the Astronomical Observatory Skalnaté Pleso*, 38, 519
- Bazin, C., Vilinga, J., Wittich, R., et al. 2015, in *SF2A-2015: Proceedings of the Annual Meeting of the French Society of Astronomy and Astrophysics*, eds. F. Martins, S. Boissier, V. Buat, L. Cambrésy, & P. Petit, 259
- Dani, T., Priyatikanto, R., & Rachman, A. 2016, in *International Symposium on Sun, Earth and Life*, arXiv:1610.07704
- Dorotovic, I., Lukac, B., Minarovjech, M., et al. 1999, *Contributions of the Astronomical Observatory Skalnaté Pleso*, 28, 224
- Espenak, F. 1989, *Fifty Year Canon of Solar Eclipses: 1986–2035*, ed. (Cambridge, MA: Sky Publishing Corporation)
- Foukal, P. V. 2004, *Solar Astrophysics*, 2nd, Revised Edition (Weinheim: Wiley-VCH), 480
- Golub, L., & Pasachoff, J. M. 2009, *The Solar Corona* (Cambridge: Cambridge Univ. Press)
- Gulyaev, R. A. 1997, *Astronomical and Astrophysical Transactions*, 13, 137
- Hanaoka, Y., Kikuta, Y., Nakazawa, J., Ohnishi, K., & Shiota, K. 2012, *Sol. Phys.*, 279, 75
- Lebecq, C., Koutchmy, S., & Stellmacher, G. 1985, *A&A*, 152, 157
- Loucif, M. L., & Koutchmy, S. 1989, *A&AS*, 77, 45
- Ludendorff, H. 1928, *itzungsber. Preuss. Akad. Wiss. Phys.-Math. Kl.*, 16, 185
- Newkirk, Jr., G. 1967, *ARA&A*, 5, 213
- Nikolsky, G. 1956, *Astronomicheskii Zhurnal*, 33, 84
- Pasachoff, J. M., Rušin, V., Druckmüller, M., & Saniga, M. 2007, *ApJ*, 665, 824
- Pasachoff, J. M., Rušin, V., Druckmüller, M., et al. 2009, *ApJ*, 702, 1297
- Pasachoff, J. M., Rušin, V., Saniga, M., Druckmüllerová, H., & Babcock, B. A. 2011a, *ApJ*, 742, 29
- Pasachoff, J. M., Rušin, V., Druckmüllerová, H., et al. 2011b, *ApJ*, 734, 114
- Pasachoff, J. M., Rušin, V., Saniga, M., et al. 2015, *ApJ*, 800, 90
- Pinter, T., Lorenc, M., Lukac, B., et al. 1997, *Contributions of the Astronomical Observatory Skalnaté Pleso*, 27, 115
- Pishkalo, M. I. 2011, *Sol. Phys.*, 270, 347
- Pishkalo, M. I., & Sadovenko, E. V. 2008, *Kinematics and Physics of Celestial Bodies*, 24, 44
- Pishkalo, N. I., & Baransky, A. R. 2009, *Kinematics and Physics of Celestial Bodies*, 25, 315
- Reginald, N. L., Cyr, O. C. S., Davila, J. M., & Brosius, J. W. 2003, *ApJ*, 599, 596
- Rusin, V., Klocok, L., Minarovjech, M., & Rybansky, M. 1996, *Contributions of the Astronomical Observatory Skalnaté Pleso*, 26, 37
- Skomorovsky, V. I., Trifonov, V. D., Mashnich, G. P., et al. 2012, *Sol. Phys.*, 277, 267
- Stoeva, P., Stoev, A., Kuzin, S., et al. 2008, *Journal of Atmospheric and Solar-Terrestrial Physics*, 70, 414
- Sýkora, J., Badalyan, O. G., & Obridko, V. N. 2003, *Sol. Phys.*, 212, 301
- Sykora, J., Badalyan, O. G., Obridko, V. N., & Pinter, T. 1999, *Contributions of the Astronomical Observatory Skalnaté Pleso*, 29, 89
- Tlatov, A. G. 2010, *A&A*, 522, A27